Journal of Molecular Liquids 241 (2017) 301–307

Contents lists available at ScienceDirect

Journal of Molecular Liquids

journal homepage: www.elsevier.com/locate/molliq

# Phase behavior of water-mediated protic ionic liquid: Ethylammonium nitrate

Hiroshi Abe [a],*, Masami Aono [a], Takahiro Takekiyo [b], Yukihiro Yoshimura [b], Akio Shimizu [c]

[a] *Department of Materials Science and Engineering, National Defense Academy, Hashirimizu 1-10-20, Yokosuka, 239-8686, Japan*
[b] *Department of Applied Chemistry, National Defense Academy, Hashirimizu 1-10-20, Yokosuka 239-8686, Japan*
[c] *Graduate School of Environmental Engineering for Symbiosis, Soka University, Hachioji, Tokyo 192-8577, Japan*

ARTICLE INFO

*Article history:*
Received 21 April 2017
Accepted 31 May 2017
Available online xxxx

*Keywords:*
Multiple pathways of crystallization
Protic ionic liquids
Crystal polymorph
Bifurcation point
Water-mediated anomaly

ABSTRACT

In pure ethylammonium nitrate (EAN), which is a protic ionic liquid (pIL), multiple crystallization pathways are extracted by simultaneous X-ray diffraction and differential scanning calorimetry measurements. Multiple pathways for crystallization are selected by minimum temperatures in a pure EAN crystal. In an EAN – water system, phase equilibria are determined precisely by *in situ* observations made by using simultaneous measurements. Electrochemical instabilities induced by proton transfer are observed at $70 < x < 90$ mol% $H_2O$ [*Chem. Phys.* **475** (2016) 119.]. Complicated phase diagrams indicate water-mediated anomalies as a crossover point from pIL-dominant to water-dominant regions.

## 1. Introduction

Low melting ionic liquids (ILs) have a big impact on conventional physical chemistry [1,2] and enlarge the possibilities of green chemistry [3,4]. Not only the pure ILs but also the IL-based mixtures have been widely investigated with regards to fundamental solubility and liquid-liquid phase equilibria [5–10]. Based on the solution properties, cost-cutting for industrial applications is done by diluting the ILs. For instance, the electrochemical properties of electric double-layer capacitors [11] and $CO_2$ capture at ambient temperature and pressure [12] are improved in binary systems rather than in pure ILs.

Proton transfer in protic ionic liquids (pILs) was characterized based on the Walden rule and compared with other solution systems [13]. Proton transfer of various types of pILs was investigated with respect to the free-energy level, which is related to the glass-transition temperature [14]. The intermediate electrochemical gap of the pILs suggests that proton transfer is described by a Grotthuss-type exchange mechanism [15]. On the other hand, the liquid structure of ethylammonium nitrate (EAN) as one of pILs was precisely estimated by neutron diffraction and empirical potential structure refinement (EPSR), where EAN was partially deuterated to obtain H-D contrast in neutrons [16]. A sponge-like nanostructure was visualized in the simulation box. Conversely, the crystal structure provides a molecular interaction, which is indicated by positional and orientational orders in the unit cell. The crystal structures of pILs are modified, reflecting the proton anomalies in spite of the simple molecular system. For EAN crystal, molecular array of $NO_3$ is modulated in unit cell. The modulation is derived from $-NH_3$ of the cation, where the proton-mediated interaction develops over the medium range [17]. The space group of EAN crystals is monoclinic, $P2_1/c$. Based on the structural features of pILs, their properties for applications are summarized in recent literature [18,19].

The thermodynamic properties were investigated systematically not only in pure EAN but also in EAN-water systems [20]. Furthermore, very recently, electrochemical proton anomalies in mixtures were reported [21]. Water-mediated electrochemical anomalies were clarified by *p*H oscillations and AC impedance spectroscopy in the water-rich region. Particularly in *p*H measurements, rhythmic *p*H oscillations in the EAN-$H_2O$ mixtures were detected only at $70 < x < 90$ mol% $H_2O$ [21]. Moreover, the specific mode of collective proton transfer was observed in the high-frequency region on the AC impedance spectra. With decreasing temperature, the conductivity decreases gradually; this is reflected by the suppression of thermally activated proton transfer. In the EAN-water system [22], the liquid structure was also investigated in the same manner as for the pure system. Data analysis of EPSR can reveal anisotropic probability distributions of molecule in the first nearest neighbor. In addition, simulations indicate that water distributes within the sponge-like structure of EAN. A water-mediated network such as cation-water and anion-water was reconstructed in the snapshot. Not only in pILs but also in aprotic ionic liquids (apILs), electrochemical anomalies were induced by adding water [23,24]. The apIL is *N*, *N*-diethyl-*N*-methyl-*N*-(2-methoxyethyl)ammonium tetrafluoroborate, [DEME][$BF_4$]. In the water-rich region of [DEME]-$H_2O$ system, rhythmic oscillations of *p*H appeared. Moreover, it was found that, in the

---

* Corresponding author.
*E-mail address:* ab@nda.ac.jp (H. Abe).

http://dx.doi.org/10.1016/j.molliq.2017.05.150
0167-7322/

[DEME][$BF_4$]-$H_2O$, water-mediated anomalous conducting mode at the specific frequency was detected by AC impedance spectroscopy [25]. Electrochemical instability of [DEME][$BF_4$]-water has a relation with medium-range order, which is detected by prepeaks in the X-ray diffraction patterns [26].

In this study, multiple pathways of crystallization of pure EAN are detected by simultaneous X-ray diffraction and differential scanning calorimetry (DSC) measurements. In the EAN-water system, phase diagrams both upon cooling and heating are determined by *in situ* observations. In the water-rich region, crystallization temperatures are widely distributed, even at the same cooling rate, and solid phases are not identified uniquely in each thermal cycle.

## 2. Experimental section

Hydrophilic EAN (98%, Kanto Chemical Co.) was selected for the sample of pIL because of its simple molecular structure, and distilled water (Kanto Chemical Co.) was used as additive. Mixtures were prepared inside a glove box through which helium gas is flowed and in which relative humidity was suppressed below 10% using silica gel.

*In situ* X-ray diffraction and DSC (SmartLab, Rigaku Co.) can probe microscopic and macroscopic phase changes. Simultaneous measurements of X-ray diffraction and DSC can determine complicated phase diagrams more precisely by removing ambiguity. For liquid materials, a vertical goniometer was indispensable to hold the sample stage horizontal. A one-dimensional detector (D/teX, Rigaku Co.) was integrated into the diffractometer for rapid scanning. The incident wavelength of X-ray was Cu Kα ($\lambda = 1.542$ Å). Dry nitrogen gas was flowed through the DSC attachment. The temperature range of the simultaneous measurements was 50 to −100 °C, and the cooling and heating rates were 5 °C/min. Crystal structure was analyzed by a combination of *FOX* [27] and *Conograph* [28]. First, possible lattice parameters were calculated by *Conograph*, following which global optimization by *FOX* identified the space group.

## 3. Results and discussion

### 3.1. Multiple crystallization pathways of pure ethylammonium nitrate

Simultaneous X-ray and DSC measurements form a quite powerful method to determine complicated phase diagrams. For instance, in pure EAN, the temperature dependence of X-ray diffraction patterns and DSC thermographs is obtained by using cooling or heating rates of 5 °C/min (Fig. 1). The open circles in Fig. 1 reveal Bragg reflections from Al, from which the sample container was made. The small peak shown by the open square in Fig. 1 represents scattering from the inner shroud of DSC. Upon cooling, we easily detect crystallization (α phase) from by the appearance of sharp Bragg reflections and an exothermal peak on the DSC thermal trace. The crystallization temperature ($T_{C1}$) is found to be −14.8 °C. The α-phase crystal structure is not identified to be $P2_1/c$, which is determined by single-crystal X-ray diffraction method [17]. One of possible space groups of the α phase is found to be triclinic ($P\overline{1}$), as listed in Table 1 and Supporting Information (Fig. S1). Upon further cooling, a quite small exothermal peak appears at −66 °C ($T_{C2}$). The X-ray diffraction pattern, however, changes little. Here we call the minor modified phase below $T_{C2}$ the α′ phase.

Upon heating, crystal-crystal phase transition occurs at −51 °C ($T_{C3}$) with exothermal peak on the DSC trace. Moreover, the X-ray diffraction pattern above $T_{C3}$ differs significantly from that of the α′ phase. Therefore, the α′ phase (green curves) transforms to the new phase (β′ phase; red curves in Fig. 1). The crystal structure of the β′ phase is determined to be monoclinic $P2_1/c$, which is exactly the same as the previously reported crystal structure (Table 1 and Fig. S1) [17]. The density of the α′ phase in this study is comparable for that of the β′ phase at low temperature [17]. For comparison, the liquid density of pure EAN at room temperature is 1.216 g/cm$^3$[18,20].

Upon increasing temperature, a weak endothermal peak appears at −41 °C ($T_{m1}$) with no change of X-ray diffraction pattern. This means that pure EAN crystal does not melt at $T_{m1}$. In a previous study dealing with heating [17], the weak peak at −42 °C was reported to be related to the melting point of $HNO_3$. In general, pure $HNO_3$ crystallizes at −41.6 °C [29]. The crystal structure of pure $HNO_3$ is monoclinic $P2_1/a$ and has a unit cell with dimensions $a = 16.230$ Å, $b = 8.570$ Å, $c = 6.310$ Å, with $\beta = 90.0°$, $Z = 16$. A weak endothermal peak at $T_{m1}$ implies that a small volume for the $HNO_3$ crystal melted in the nonmelting EAN crystal (β′ → β). If we extend this small amount of melting into cooling process, the small exothermal peak upon cooling means a small amount of $HNO_3$ crystallization at $T_{C2}$ (α → α′). Also, enthalpy changes both of weak peaks are comparable. Here, we assume that the small exothermal and endothermal peaks correspond to crystallization and melting of $HNO_3$, respectively. Density functional theory (DFT) calculations raise the possibility of partial crystallization of $HNO_3$ in pure

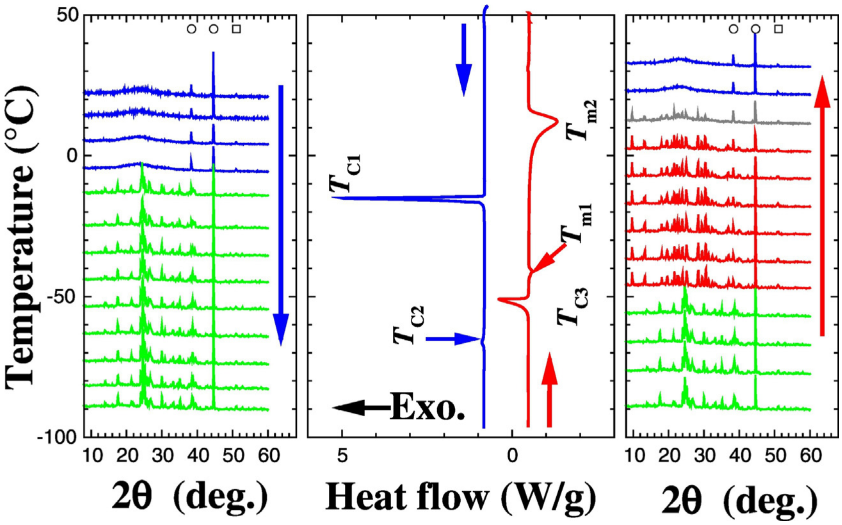

**Fig. 1.** X-ray diffraction patterns and DSC thermal traces obtained by simultaneous measurements. $T_{C1}$, $T_{C2}$, $T_{C3}$, $T_{m1}$, and $T_{m2}$ are the crystallization temperatures of EAN and $HNO_3$, crystal-crystal phase transition temperature, melting points of $HNO_3$ and EAN, respectively. The blue curves represent X-ray diffraction patterns in the liquid state. α and α′ phases are shown by the green curves, whereas β and β′ phases are shown by the red curves. Open circles indicate Bragg refractions from Al, from which the sample container is made. Open squares correspond to the peak scattered from the inner shroud of DSC. (For interpretation of the references to colour in this figure legend, the reader is referred to the web version of this article.)